Electronic Supplementary Material (ESI) for Nanoscale.
This journal is © The Royal Society of Chemistry 2018

Supporting information

Time-dependent luminescence loss of individual upconversion nanoparticles upon dilution in aqueous solutions

Oleksii Dukhno[1], Frederic Przybilla[1], Verena Muhr[2], Markus Buchner[2], Thomas Hirsch[2] and Yves Mely[1*]*

1) Laboratory of Biomaging and Pathologies, UMR 7021 CNRS, University of Strasbourg, 67000 Strasbourg, France
2) Institute of Analytical Chemistry, Chemo- and Biosensors, University of Regensburg, 93040 Regensburg, Germany

* *Corresponding authors:* oleksii.dukhno@unistra.fr, yves.mely@unistra.fr

Experimental methods

Materials and synthesis. Reagents and solvents were purchased from Sigma-Aldrich and used without further purification. Water for all experiments was purified with a Merck Millipore Milli-Q system.

Oleate-coated UCNPs were prepared and characterized (Fig. S1) as described in Wilhelm et al. 2015.[1] To render the UCNP hydrophilic and thus, water dispersible, N-dodecyl-polyisobutylene-alt-maleamic acid (PMA) was synthesized and used to coat the UCNPs, as described in Dukhno et al.[2] After coating, the particles were purified by centrifugation (12000 g RCF, 4°C, 1 h) and pellet redispersion in 10 mM NaOH with 1 mM NaF. This treatment was performed twice to ensure removal of empty polymer micelles. Quality control was done by DLS measurements.

XRD patterns were recorded on a Huber Guinier G670 diffractometer with a Kα-Cu source (λ = 1.54060 Å). *TEM images* were acquired with a 120 kV Philips CM12 microscope on carbon-coated copper grids and were analyzed with ImageJ and Origin.

DLS measurements were performed on a Malvern Zetasizer Nano instrument to characterize the size of the polymer-coated UCNPs in Brand plastic cuvettes (lot #759015). Correlation curves for each sample were accumulated 3 times. Treatment parameters were normal resolution and size distribution by volume.

Theoretical estimation of the extent of particle degradation

A typical stock dispersion of water-dispersed UCNPs after synthesis and coating contains ~1 mg/mL of material.[2,3] Knowing the density of β-$NaYF_4$ (4.21 g/cm^3) and the volume of a spherical 30 nm particle (14137 nm^3) we can calculate that the particle concentration is 1.68×10^{13} particles per mL, or ~28 nM. β-$NaYF_4$ unit cell volume is 107 A^3, so a UCNP 30 nm in diameter contains ~132000 unit cells. Knowing the particle concentration and the amount of unit cells per particle, we can estimate the total amount of ions trapped inside the particles, which is 3.7 mM for Na^+, 3.7 mM for Y^{3+}, and 14.8 mM for F^-.

Next, we calculated the concentration of ions in water over saturated $NaYF_4$ and YF_3 from their solubility products.[3,4] The calculation for YF_3 is necessary because its overall solubility is lower than for $NaYF_4$, so the dissolution could potentially proceed through YF_3 as an intermediate.

$$NaYF_4(s) + H_2O \rightleftharpoons Na^+_{aq} + Y^{3+}_{aq} + 4\,F^-_{aq}$$
$$K_s(NaYF_4, pH\ 7) = [Na^+][Y^{3+}][F^-]^4 = 1.6 * 10^{-26}\ M^6$$
$$[Na^+] = 20\,\mu M\ ; [Y^{3+}] = 20\,\mu M\ ; [F^-] = 80\,\mu M$$

$$YF_3(s) + H_2O \rightleftharpoons Y^{3+}_{aq} + 3\,F^-_{aq}$$
$$K_s(YF_3, pH\ 7) = [Y^{3+}][F^-]^3 = 3.98 * 10^{-19}\ M^4$$
$$[Y^{3+}] = 11\,\mu M\ ; [F^-] = 33\,\mu M$$

The saturated concentrations for lanthanide ions are 180-340 times larger than the concentration of ions trapped inside the particles. This implies that in the stock dispersion, the particles only lose ~0.3-0.5% of total material before reaching the solubility equilibrium.
Meanwhile, in single-particle microscopy conditions, particles are typically attached to their target substrates (e.g. coated glass surfaces or cells), with nearly no particles present in dispersion. For a typical single-particle imaging setup with a 100x magnification objective, a good separation of individual particle spots on microscopy image requires approximately 100 particles per region of interest of 20×20 μm^2. For a microscopy well plate with a well surface of 1 cm^2, this corresponds to 25 million particles per well. The wells themselves are filled with 300 μL aqueous buffer. Thus, the *effective* concentration of immobilized particles in microscopy wells is ~140 fM. Again, knowing the particle concentration and the amount of unit cells per particle, the total amount of ions trapped inside the particles can be estimated at 18.5 nM for Na^+, 18.5 nM for Y^{3+}, and 74 nM for F^-. These concentrations are much lower than the concentrations for the saturated solution, meaning that from a thermodynamical standpoint, the particles are expected to dissolve completely. Meanwhile, the kinetics of their dissolution depend on the accessibility of the particle surfaces to the aqueous phase.

Characterization of oleate-capped UCNPs after synthesis

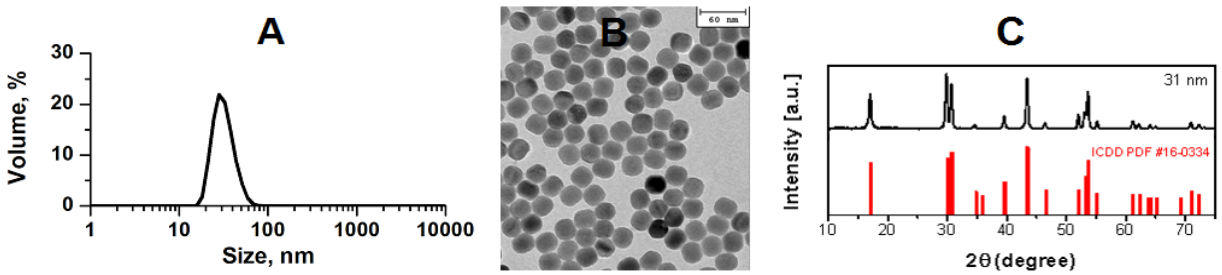

*Figure S1. Characterization of the oleate-capped UCNPs (*β-$NaYF_4$: 20%Yb, 2%Er*) after synthesis. The UCNPs were characterized by A: DLS in cyclohexane. B: TEM and C: XRD. The XRD pattern of the nanocrystals (black) is compared to the corresponding standard pattern of hexagonal phase $NaYF_4$ (red, ICDD PDF #16-0334).*

Cuvette measurements of UCNP dispersions in 1 cm BRAND plastic cuvettes (Cat. No. 7590-15) were performed with a homemade setup (Fig. S2). Excitation at 980 nm was provided by a continuous-wave laser coupled to a single mode fiber with a maximum output of 350 mW (Qphotonics, QFBGLD-980-350). Excitation light was focused in the cuvette by a lens of 100 mm focal distance. Excitation power inside the cuvette was calculated to be 6.2 kW/cm^2 (see below). The scattered/reemitted laser light was removed by a low pass filter (Semrock, E700SP). The emission was collected through a monochromator (Jobin Yvon HC10IR) with an avalanche

photodiode (Excelitas SPCM-AQRH-16). Spectrometry was performed with an identical optical path for excitation, with emission collected by a fiber spectrometer (Avaspec ULS3648).

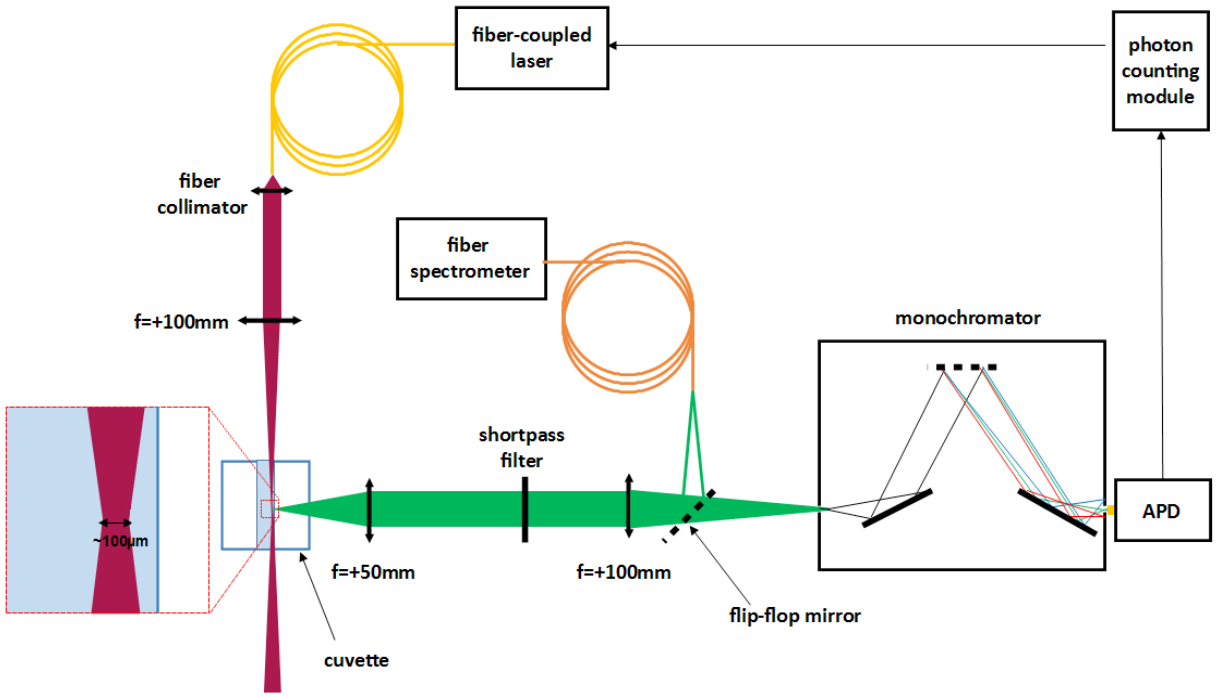

Figure S2. Scheme of the setup for cuvette measurements.

To estimate the excitation intensity within the cuvette, the laser beam intensity profile was experimentally measured inside the cuvette by the knife-edge technique, using a razor blade (~2 mm wide).[5] Briefly, the blade was glued on a thin steel rod, mounted on a two axis micrometer translation stage (Thorlabs PT1A/M), and immersed in the cuvette filled with deionized water. This setup allows to achieve a bidirectional motion, along the beam and vertically (Fig. S3, A). Through the vertical movement, the razorblade progressively occludes the beam and thus, the beam power collected by the detector (Newport 1917R power meter) gets lower. By repeating the measurement at different depths in the cuvette, a full beam blade occlusion profile can be collected (Fig. S3, B), from which the beam geometry can be calculated. For our calculations, the beam geometry was considered to be Gaussian and circular (with no ellipticity). To correct for water absorption, we compared the intensity of the transmitted beam with an empty cuvette and after filling the cuvette with water. We found the water absorption to be non-negligible, at a value of 0.191 cm^{-1}. By knowing the beam geometry and beam attenuation by the medium, the full excitation profile (Fig. S3, C) and thus, the beam waist radius (30.6 µm) and the average excitation intensity in the beam waist (6.2 kW/cm^2) can be estimated. Calculations were performed in Wolfram Mathematica 11.0.

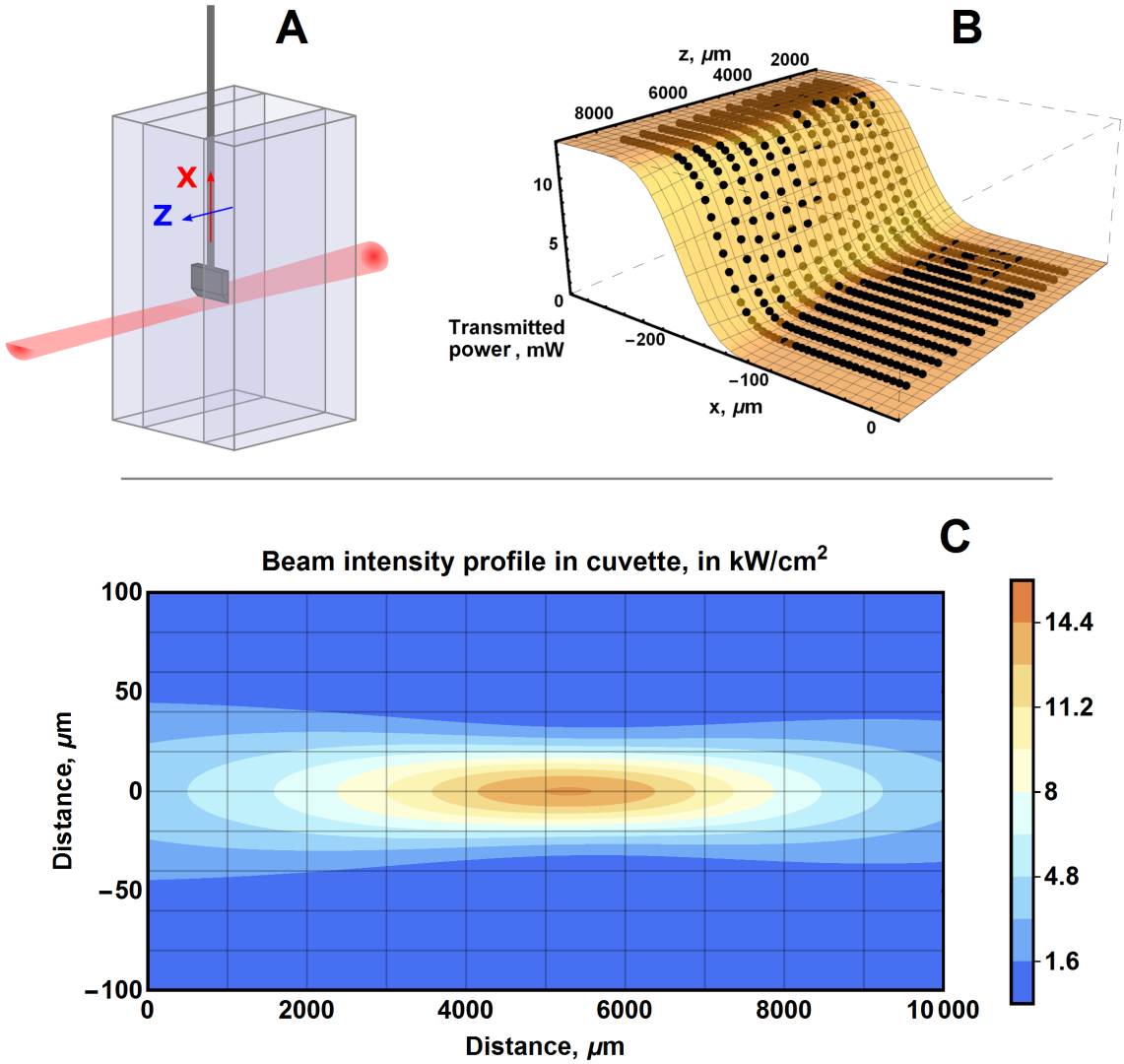

Figure S3. Measurement of the excitation beam intensity profile for the cuvette setup. A: setup for measuring the beam profile. The laser beam is occluded by a movable razor blade, permitting only a part of the beam to go through. B: dependence of the transmitted power on lateral and vertical blade position (black points) and its global fit with the occlusion curve (orange surface). C: obtained beam intensity profile that takes into account water absorption inside the cuvette.

Luminescence spectroscopy of water-dispersed UCNPs

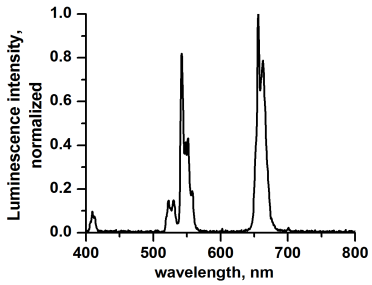

Figure S4. Luminescence spectrum of the stock solution of polymer-coated UCNPs dispersed in 1 mM NaF at an estimated particle concentration of 0.8 mg/mL. The spectrum was measured by

focusing a 980 nm laser beam in a cuvette, with a calculated excitation intensity of 6.2 kW/cm^2.

Microscopy setup and excitation intensity determination

Luminescence imaging of UCNPs was performed on an inverted microscope (Olympus IX71) equipped with a high numerical aperture objective (Olympus, UApo N 100x/1.49 Oil). A 980 nm continuous-wave laser coupled to a single mode fiber with a maximum output of 350 mW (Qphotonics, QFBGLD-980-350) was passed through a longpass filter(Chroma, E780LP) used to excite the UCNPs with an excitation power density of 8 kW/cm^2 in epi illumination. Luminescence emission was separated from the excitation beam by using a short pass dichroic mirror (Chroma, T875spxrxt), while the residual laser light was removed by a low pass filter (Chroma, E700SP). Emission was detected by an electron multiplying CCD camera (Hamamatsu, ImagEM X2 C9100-23B) through an image splitting system for simultaneous dual wavelength imaging (Hamamatsu, W-VIEW GEMINI). This splitting system was used with an appropriate dichroic mirror (Semrock, FF560-FDi01) and band pass filters for green channel (Semrock, FF01-535/50) and red channel (Semrock, FF01-660/30-25). We have calibrated the spectral response of our microscopy setup with an external white light source as a reference and used this calibration for correcting the red to green ratios. Acquisition was fully automated and controlled by scripts within the MicroManager framework.[6] All static images shown in the article were recorded as an averaged stack of 100 images, each with 100 ms exposure time.

Wide-field microscopy images were treated with ImageJ 1.51h as part of the FIJI package. Stitching was performed with the Grid/Collection stitching plugin.[7] Drift correction was done using a homemade script written in ImageJ macro language (available on request). Spot fitting was performed with the Gaussian Fit module of the GDSC SMLM package.[8] Data analysis was performed with homemade scripts written in Python 3.4.3 (available on request).

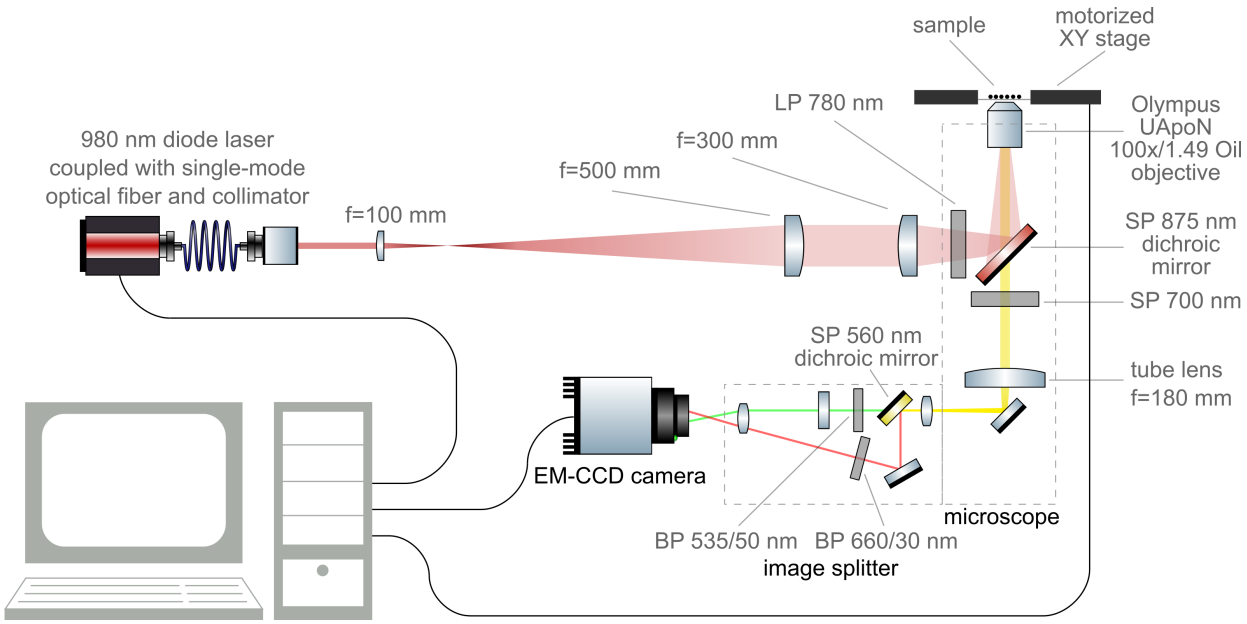

Figure S5. Scheme of the microscopy setup.

To estimate the excitation beam profile in the image plane of our microscopy setup, we imaged oleate-capped UCNPs dried at low density on a glass coverslip. A single UCNP was scanned through the field of view, using the motorized XY stage (Märzhäuser) with a step of 4 µm (Fig. S6, A). The UCNP luminescence was measured as a function of its position, which provides the excitation intensity map (Fig. S6, B). To check the dependence of the UCNP luminescence on the excitation intensity, the UCNP was positioned in the center of the excitation beam and its

luminescence was measured at various laser powers. In the high power regime used in our experiments, the luminescence of the individual UCNP in the red channel was observed to be linearly dependent on the laser power and thus, on the excitation intensity (Fig. S6, C). By fitting the intensity map with a 2D circular gaussian profile (Fig. S6, D), the beam waist radius in the image plane was found to be 28 µm. Knowing the laser power after the objective (96 mW), the average excitation intensity was found to be 8 kW/cm^2 at the center of the beam, where the excitation intensity varied by less than 10% (in a 6.3 µm radius from the beam center). Throughout the paper, we only considered the luminescence of UCNPs positioned in the center of the beam.

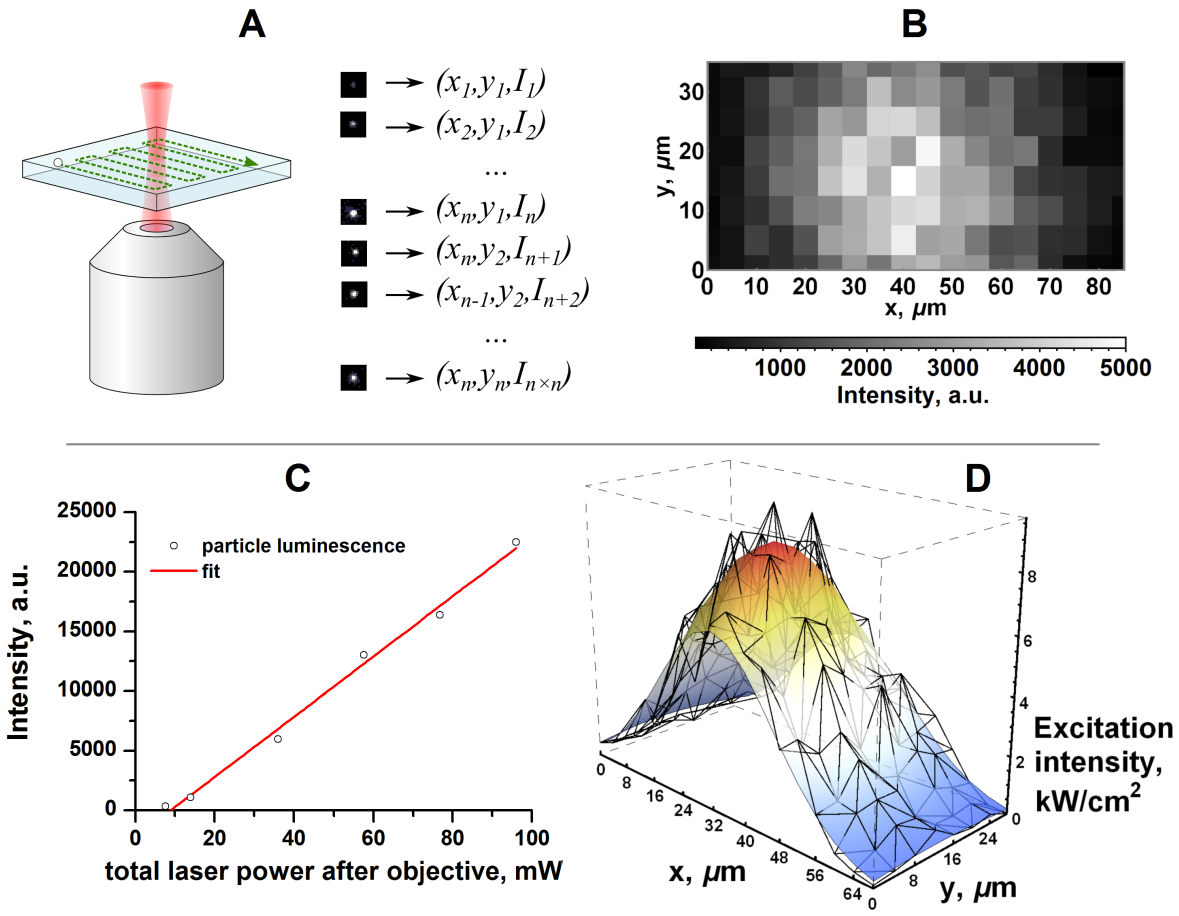

Figure S6. Measurement of the excitation beam intensity profile for the microscopy setup. A: scheme of the mapping experiment. B: excitation intensity map in the field of view. C: excitation power dependency for an immobilized particle. D: excitation beam profile at the maximum laser power.

AFM measurements were performed on a Veeco Nanoscope IIIa MultiMode AFM (Veeco, Santa Barbara, California, United States) in tapping mode, using RTESP7 cantilever probes (silicon, 300 MHz). Raw AFM data were treated with the Gwyddion 2.40 software (automatic mean plane subtraction, then automatic line correction by matching height median).
For correlated atomic force microscopy / wide-field upconversion luminescence microscopy (AFM/Upcon), the particles were 1000-fold diluted in water from stock solution and dried for 1 h in a vacuum chamber on mica glued to a thin steel washer. To ensure a clean flat surface, mica was exfoliated with a scotch tape immediately before the experiment. The bottom side of the mica was marked with a permanent marker (Staedtler permanent Lumocolor, red) to leave a spot clearly visible in bright field microscopy. The position of the scanned region of interest (ROI) relative to the marker spot was noted. Then, the sample was inverted and fixed on a glass coverslip with a

scotch tape. The marker spot was found by illuminating the sample with a white lamp, and the objective was positioned with an XY stage with corresponding offsets relative to the spot, to find the approximate position of the scanned ROI. The precise ROI was located manually afterwards. Fig. S4 illustrates the protocol.
Afterwards, the luminescence images were treated by a landmark-based rigid transformation to match the AFM geometry, using Landmark Correspondences FIJI plugin.[9] The rigid transformation was chosen to retain the spot proportions and inter-spot distances. Landmarks were set manually by the user. An AFM-Upcon image (20x20 µm) of immobilized UCNPs dried on mica is given in Fig. S5.

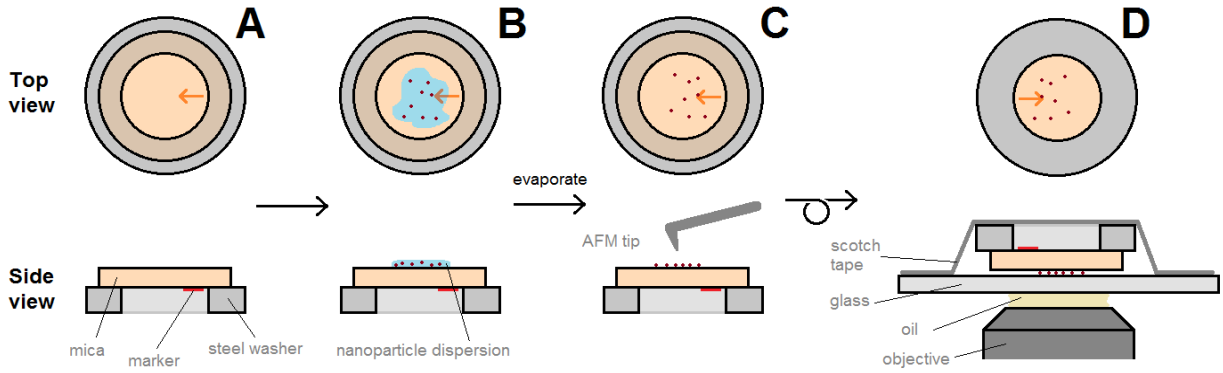

Figure S7. Sample preparation for correlated AFM/ wide-field upconversion luminescence microscopy. A: Initial assembly of mica attached to a steel washer, with a marker on the bottom side (red arrow). B: A drop of nanoparticle dispersion is added. C: After evaporation, AFM is performed on the sample. D: The sample is then inverted and fixed to a glass coverslip. The marker is located by eye in the bright field mode, and the exact ROI is located with an XY stage.

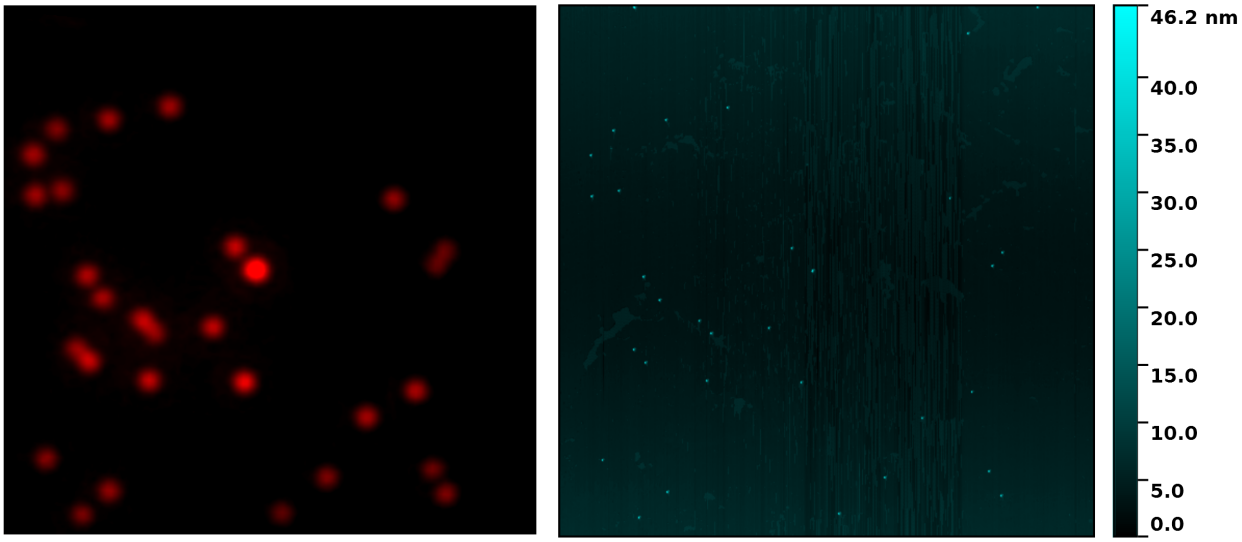

Figure S8. Full AFM-Upcon image (20×20 µm) of immobilized UCNPs dried on mica as described in Fig. S7. Red: luminescence in the red channel. Teal: sample height, as measured by AFM.

Monitoring UCNP dissolution by combined dialysis/conductometry

To directly confirm the UCNP dissolution, we performed combined dialysis/conductometry measurements to monitor the ion leakage from UCNPs in real time. To this aim, 0.4 mL of UCNP stock solution was desalted through an Illustra NAP-5 column (GE) that was equilibrated with deionized water. 0.5 mL of nanoparticle dispersion was collected, diluted to 0.6 mL and closed in a Teflon vessel capped with a SpectraPor RC 3 dialysis membrane (MWCO 3.5 KDa). The vessel was immersed in 3.5 mL deionized water with a platinized conductivity cell (Radiometer CDC 745-9), under continuous stirring. The conductivity of the dialysate was continuously measured by a conductometer (Tacussel CD 6N). After 3-16 h (see below), 1-2 mL of dialysate was replaced with deionized water and the pipetted dialysate was stored. This procedure was repeated 16 times in total.

Before the experiment, all parts of the experimental assembly were thoroughly rinsed and soaked 20 min in deionized water to avoid contamination. This procedure was performed thrice.

Throughout the experiment, the temperature was kept at 22°C. All deionized water used in the experiments was allowed to equilibrate with the atmospheric CO_2 over at least 4 h.

The scheme of the experiment is provided in Fig. S6A. For each dialysate dilution, the solution becomes sub-saturated, lowering the conductivity. Then, UCNP dissolution starts and the solution becomes saturated once more. At a certain point, when all ions escape the UCNPs and only surface coating polymers are left inside the dialysis vessel, slower kinetics of conductivity restoration are expected, as the concentration gradient decreases and dialysis rate drops.

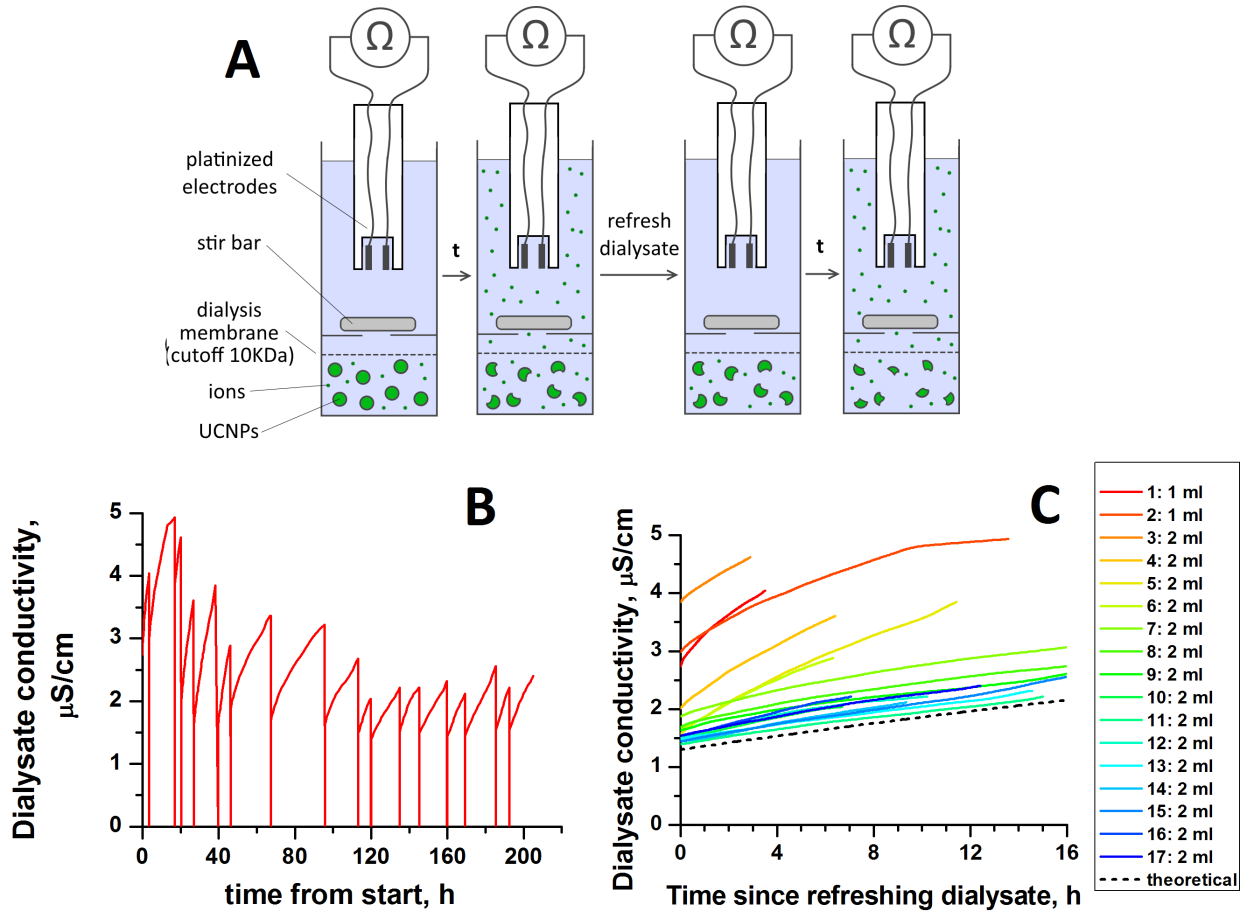

Figure S9. Monitoring UCNP dissolution by combined conductometry/dialysis. A: Schematic representation of the experiment. B: Raw conductivity curves for the full duration of the experiment. At each vertical line, a part of the dialysate was replaced by mQ water. First two cycles have been performed with substitution of 1 mL, the other ones with 2 mL. C: Conductivity restoration curves for each cycle of dialysate refreshing.

The results are shown in Fig. S6B and C. As expected, we observed a drop in conductivity for each dilution, as a result of the solution becoming sub-saturated in UCNP ions. Then, progressive UCNP dissolution restores the solution saturation again. The initial curves show higher conductivities, likely corresponding to the relatively fast diffusion of highly soluble NaF into the dialysate and formation of less soluble YF_3 on particle surfaces exposed to water. The kinetics of conductivity restoration become progressively slower at each dilution. At a certain point, when all ions escape the UCNPs and only surface coating polymers are left inside the dialysis vessel, slower kinetics of conductivity restoration are observed, as the concentration gradient decreases and dialysis rate drops. To confirm that the membrane was intact and no UCNPs escaped the dialysis vessel during the experiment, we also performed upconversion luminescence measurements in cuvette and found no detectable luminescence in any of the collected dialysates. Comparing the luminescence of the dialysis vessel content to the initial stock solution, we found a 36000-fold loss in luminescence intensity, i.e. 99.997% of signal was lost. Overall, these data are a direct proof of ion leakage from UCNPs.

We also performed a theoretical estimation of conductivity restoration. We assumed that after several dialysis cycles, YF_3 is the dominant solid phase at equilibrium, as it has the lowest known solubility product among the solid phases that consist of the combinations of Na^+, Y^{3+}, Yb^{3+}, Er^{3+} and F^-,[4,10] and thus will be the last one to dissolve. We also assumed that hydrated Yb^{3+} and Er^{3+} are equal to Y^{3+} in terms of their mobility and molar conductivity.[11]

Next, we calculated the concentration of ions in water over saturated YF_3 from its solubility product[4]:

$$YF_3(s) + H_2O \rightleftharpoons Y^{3+}_{aq} + 3F^-_{aq}$$

$$pK_s(YF_3) = 18.4;\ K_s(YF_3) = [Y^{3+}][F^-]^3 = 3.98 * 10^{-19};\ 3[Y^{3+}] = [F^-]$$

$$[Y^{3+}] = 11\,\mu M;\ [F^-] = 33\,\mu M$$

Meanwhile, YbF_3 has higher solubility[9]:

$$pK_s(YbF_3) = 16.6;\ [Yb^{3+}] = 31\,\mu M;\ [F^-] = 93\,\mu M$$

This implies that, similar to Na^+, Yb^{3+} ions are removed faster than Y^{3+}.
The influence of ErF_3 can be neglected, as it represents only 2% of lanthanide composition in our UCNPs and has a $pK_s(ErF_3)$=17.5, in between YF_3 and YbF_3.

Next, we calculated the concentration of Y^{3+} and F^- in the dialysate as a function of time. For this, we made following assumptions:
1) The rate limiting step in mass transport at such concentrations is diffusion. The dissolution process is assumed to be faster, even when a large proportion of UCNP surface is shielded by coating. Diffusion is assumed to follow Fick's laws.[12]
2) Solid phase dissolves faster than ion transport occurs, so the ion concentration inside the dialysis vessel is constant, and changes only in the dialysate.
3) Both compartments separated by the membrane are mixed much faster than diffusion occurs. Thus, diffusion *through membrane* is considered to be the rate limiting step.
4) Charge effects and transmembrane potentials arising from the difference in ion concentrations inside and outside of the dialysis vessel are neglected. Both inner and outer solutions are considered

to be neutral, so conservation of charge requires diffusion to be limited by the diffusion of the slowest ion (Y^{3+} with diffusion coefficient of 5.5×10^{-10} m^2/s in water at 298 K [13]). This is a reasonable assumption for such highly diluted solutions.
5) No polymer coating or solid phase is expected to escape through membrane into the dialysate. This is a reasonable assumption, as free polymers tend to assemble in micelles of about 10 nm in size,[2] and the MWCO of membrane is more than 4 times lower than the average mass of individual polymer chains.
6) The dispersion of UCNPs has already reached a dissolution equilibrium at the start of the experiment.
7) The permeability coefficient (K) of regenerated cellulose for small inorganic ions is assumed to be 0.2. Values for the Spectra/Por membrane used in this study are not openly available, but a literature survey for a set of commercially available regenerated cellulose membranes[14] suggests that their permeability for small inorganic ions is very similar.

From these assumptions, we obtained the following system of parameters and differential equations:

$$C(Y^{3+})_{\text{UCNP dispersion}} = 11\ \mu\text{M} = constant$$
$$C(F^{-})_{\text{UCNP dispersion}} = 33\ \mu\text{M} = constant$$
$$\frac{\partial}{\partial t}C(Y^{3+})_{\text{dialysate}} = \frac{KAD}{l}\left(C(Y^{3+})_{\text{UCNP dispersion}} - C(Y^{3+})_{\text{dialysate}}\right)$$
$$\frac{\partial}{\partial t}C(F^{-})_{\text{dialysate}} = \frac{KAD}{l}\left(C(F^{-})_{\text{UCNP dispersion}} - C(F^{-})_{\text{dialysate}}\right)$$
$$K = 0.2;\ A = 1.32\ cm^2;\ D = 5.5 * 10^{-10}\ m^2\ s^{-1};\ l = 1\ mm$$

To calculate the conductivity, we use an infinite dilution approximation, which is reasonable for our concentrations. The conductivity of the dialysate can be expressed from the Kohlrausch law as:

$$G = \sum_i z_i \lambda_i C_i = 3\lambda^{+}(Y^{3+})C(Y^{3+})_{\text{dialysate}} + \lambda^{-}(F^{-})C(F^{-})_{\text{dialysate}}$$

where λ are the ionic conductivityies at infinite dilution for the respective ions at 298 K.

Considering that mQ water is in equilibrium with atmospheric CO_2 (which doesn't substantially influence YF_3 dissolution), we obtain a final expression for conductivity:

$$G = G_{\text{mQ + CO}_2} + 3\lambda^{+}(Y^{3+})C(Y^{3+})_{\text{dialysate}} + \lambda^{-}(F^{-})C(F^{-})_{\text{dialysate}}$$
$$G_{\text{mQ + CO}_2} = 1.5\ \mu S\ cm^{-2}$$

The conductivity of mQ water in equilibrium with atmospheric CO_2 was measured experimentally using the aforementioned setup.

By solving the system of differential equations for the dialysate concentration over time, the theoretical curve for the conductivity dependence over time could be calculated (Fig. S6C). Calculations were performed in Wolfram Mathematica 11.0. Calculation file is available upon request.

Large-ROI microscopy: effect of illumination, correlation of initial intensity and luminescence loss

To confirm that the dissolution of UCNPs does not only happen in the sample volume that is continuously illuminated by the laser, we immobilized UCNPs on PEI in the presence of 1 mM NaF as described above. First, 49 (7×7) individual images of the sample luminescence were taken every 20 μm and stitched into a large ROI. Then, the well was flushed thrice with mQ water and incubated in the dark for 150 min. Finally, the well was flushed thrice with 1 mM NaF and the imaging procedure was repeated.

Raw images are shown on Fig. S7A and B. Images of the highlighted region before and after incubation with water are provided on Fig S7C. Similarly to luminescence homogeneity tests, spots were fitted with free-angle 2D elliptic Gaussian. The intensity histograms were built for all spots and for diffraction-limited spots (Fig. S7D and E).

A total disappearance of the luminescence for most particles and a strong decrease for others were observed. Specifically, from 5458 particle spots (3189 taken as diffraction-limited) only 1342 (990) retained significant luminescence. Taking the luminescence intensity of the disappeared spots as zero, the overall luminescence loss of the sample was found to be 88% (82% for the diffraction-limited spots), similar to the measurements on a small ROI performed under continuous illumination. Thus, we conclude that continuous laser illumination did not affect the dissolution kinetics of our sample and that it occurred in the same way across illuminated and unlit sample regions.

To find out whether the extent of luminescence loss could be predicted from initial particle intensity, we correlated initial particle intensity with its luminescence loss after 150 min in water. This correlation was performed for all particles in the sample (Fig. S7F). We observed virtually no correlation between these parameters, albeit a slight prevalence of high luminescence loss (50 to 100%) was noted for large aggregates. Thus, we conclude that the extent of luminescence loss cannot be reliably predicted from the initial particle intensity.

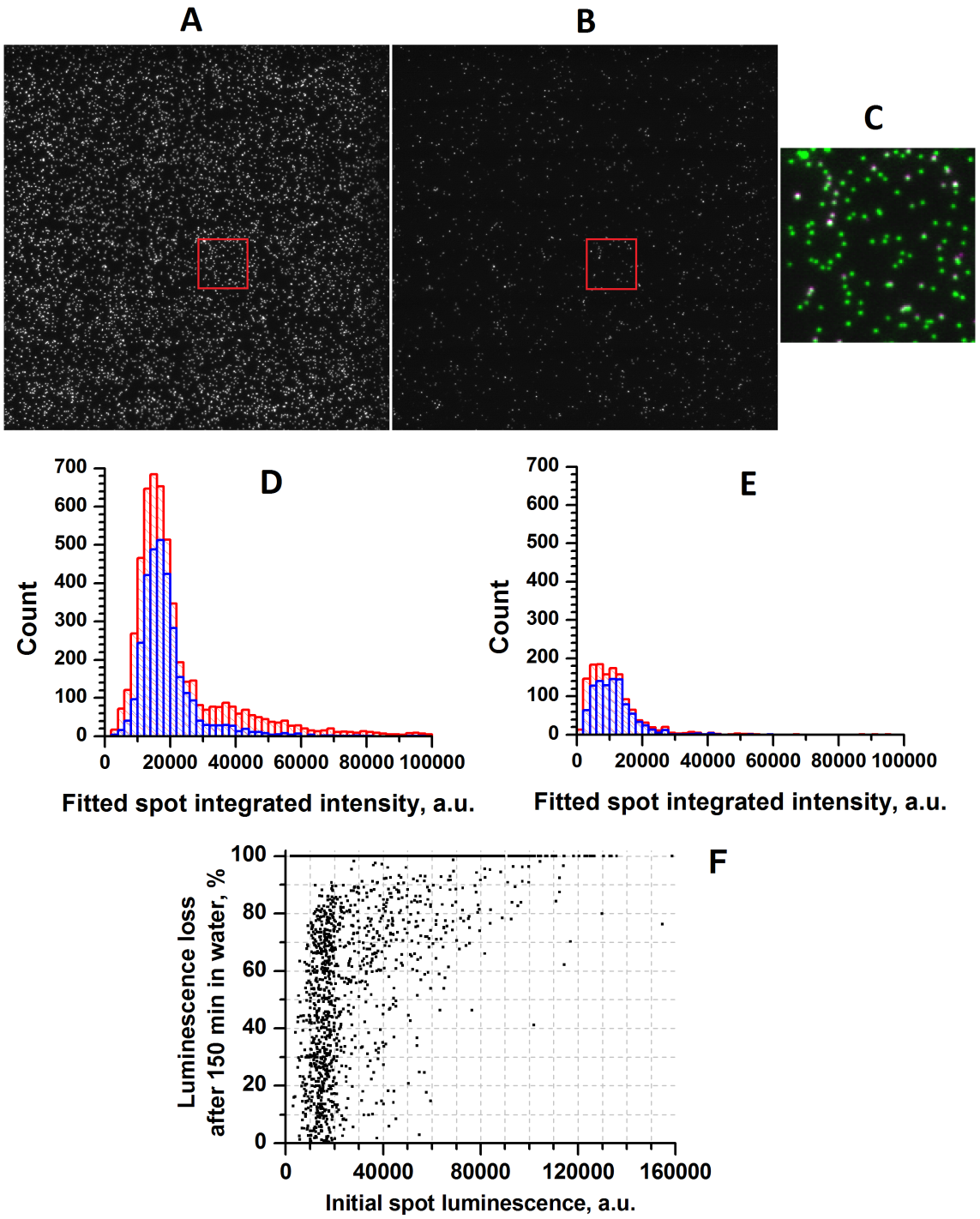

Figure S10. Wide-field imaging and size distribution of water-dispersed polymer-coated UCNPs adsorbed on a thin layer of PEI in 1 mM NaF before and after incubation for 150 min in water. A: 144×144 µm ROI in the red channel, stitched from 49 (7×7) individual wide-field images. Excitation was at 980 nm with an intensity of 8 kW/cm^2. B: Same region imaged after incubation for 150 min in water. C: Overlap of 20×20 µm boxed regions from A (green) and B (magenta). A slight shift in the positions of some particles is commonly observed after multiple flushes. D: Histogram of the integrated intensities of the 2D free-angle elliptic gaussian spot fits from image A (red) and the same histogram excluding spots that have widths more than 25% larger than the theoretical diffraction limit (blue). E: Same for image B. F: Correlation of the extent of luminescence loss and initial particle intensity.

Videomicroscopy of individual polymer-coated UCNPs in aqueous conditions was performed with the aforementioned luminescence imaging setup, using Ibidi µ-Slide 8 well glass bottom plates. First, the wells were filled with 300 µL of 1 mg/mL solution of branched polyethylenimine (PEI, Sigma-Aldrich, lot #408727) in 20 mM Tris buffer, pH 7.2. The wells were incubated for 20 min at room temperature, allowing PEI to electrostatically bind to the glass. Then, the solution was removed by a pipette and washed 2 times with 300 µL of 1 mM aqueous NaF. The stock particle dispersion was 100-fold diluted and added to the well. After 2 min of incubation, the particle dispersion was removed, and the wells with immobilized particles were washed 3 times with 300 µL of 1 mM NaF, before starting the imaging sequence. Images were taken every 30 seconds. As mechanical manipulations (e.g. washing) on the microscope stage induce local strains and movement of the microscopy oil, a focus drift was observed. To compensate, the focus was adjusted manually throughout the experiment to provide a stable diffraction-limited PSF. After 25 min, the buffer was removed from the well and the particles were washed 3 times with 300 µL of deionized water or 30 µM NaF in water. For the 1 mM NaF condition, this step was omitted. After that, the imaging sequence was continued for ~150 min. Frames that gave a consistent change of spot width for all particles were deemed "out of focus" and discarded.
Wide-field videos of UCNP luminescence over time in different conditions are available in the Supporting Information section of the website of the journal (video files labeled "dissolution_1mM_NaF_to_water.avi", "dissolution_1mM_NaF_to_NaF30uM.avi" and "dissolution_1mM_NaF_continuous.avi", corresponding to particle dissolution in water, 30 µM NaF and 1 mM NaF, respectively). Raw uncompressed image stacks in TIFF format are available on request.

Wide-field images of polymer-coated UCNPs in fluoride buffers and magnified individual particles

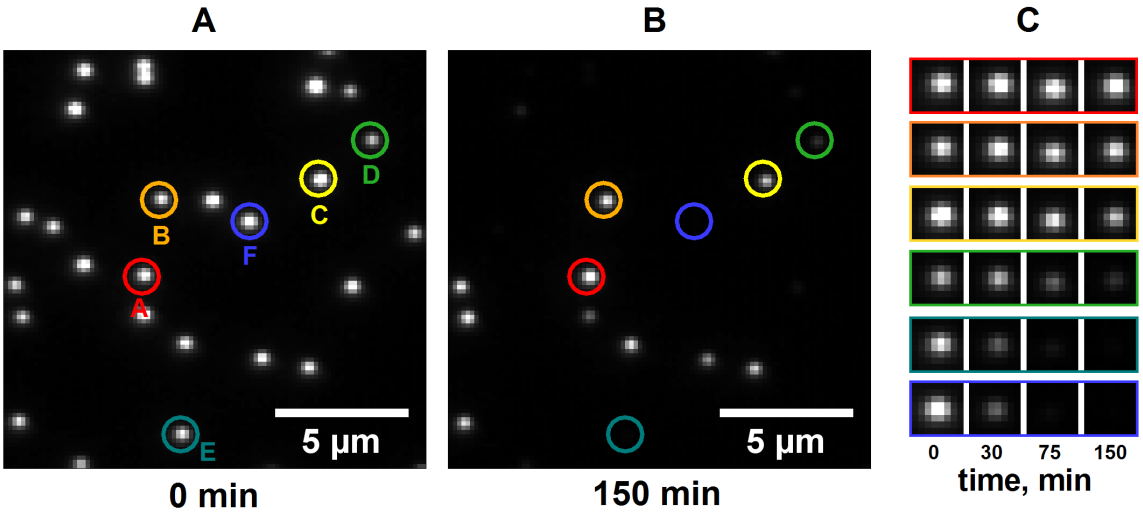

Figure S11. Luminescence over time of individual polymer-coated UCNPs in 30 µM sodium fluoride solution. Wide-field image of polymer-coated UCNPs in the red channel immediately after washing (A) and after 150 min incubation in 30 µM NaF (B), with several particles highlighted. (C) Time-dependent changes of the images of the highlighted particles (1.28×1.28 µm).

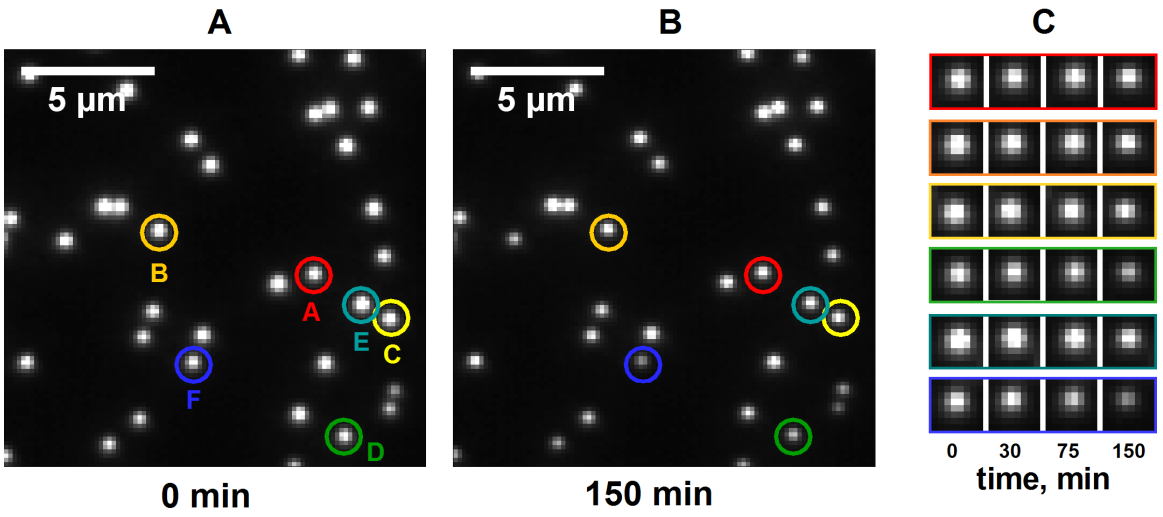

Figure S12. Luminescence over time of individual polymer-coated UCNPs in 1 mM sodium fluoride solution. Wide-field image of polymer-coated UCNPs in the red channel immediately after washing (A) and after 150 min incubation in 1 mM NaF (B), with several particles highlighted. (C) Time-dependent changes of the images of the highlighted particles (1.28×1.28 µm).

Measurements of the changes in UCNP luminescence over time in cuvette

To observe the dissolution-related effects at the ensemble level, we diluted by 100-fold the UCNP dispersions in deionized water, 30 µM NaF or 1 mM NaF, and continuously monitored the photon counts with a sensitive avalanche photodiode, using an integration time of 1 s. The results for the red and green emission intensities and the RTGR are shown in Fig. S10 (each curve is an average of two experiment repeats, smoothed with an 11-point normal-weighted rolling average).

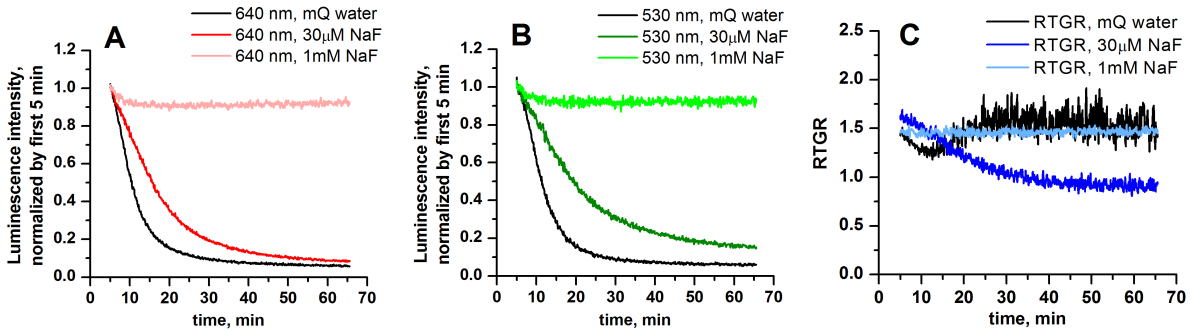

Figure S13. Cuvette measurements of the luminescence changes over time of polymer-coated UCNPs in aqueous solutions. A: red band. B: green band. C: red-to-green ratio.

Excitation intensity dependence of UCNP luminescence in the presence of 1 mM NaF

To investigate how the excitation intensity affects the UCNPs' band ratio, particles were immobilized on PEI in the presence of 1 mM NaF. The single particles in the center of the beam were illuminated with different excitation intensities by adjusting the laser power. To get a robust estimate of the RTGR values, the experiment was repeated 10 times over 30 minutes (Fig. S14, A). Focus drift was corrected by hand throughout the measurement. The particles showed a decrease in the RTGR value which correlated with the decrease in excitation intensity (Fig. S14, B).

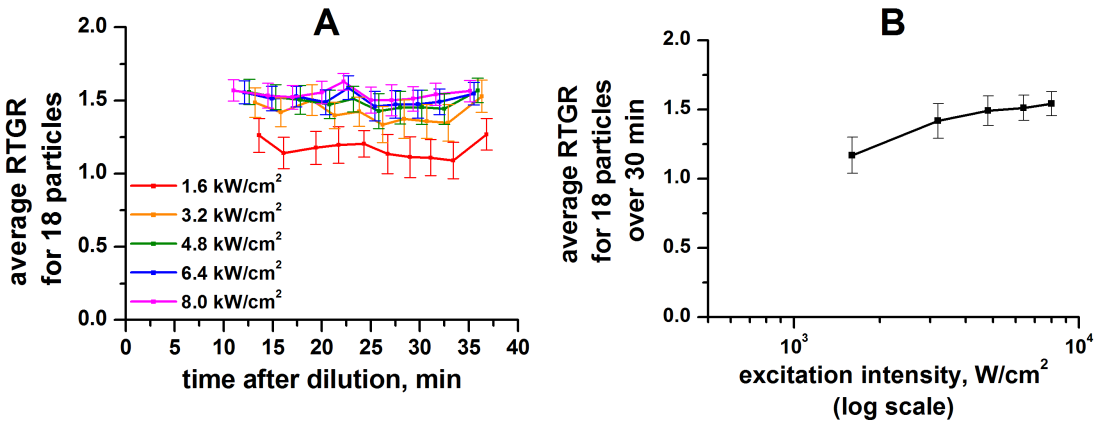

Figure S14. Excitation intensity dependence of UCNP red to green ratio (RTGR). A: Mean (+/- standard deviation) of RTGR values measured for 18 particles under different excitation intensities. Measurements were repeated 10 times over 30 minutes on the same field of view to check the stability over time. B: Average excitation intensity dependence of RTGR values, calculated as an average over 30 minutes.

References

1 S. Wilhelm, M. Kaiser, C. Würth, J. Heiland, C. Carrillo-Carrion, V. Muhr, O. S. Wolfbeis, W. J. Parak, U. Resch-Genger and T. Hirsch, *Nanoscale*, 2015, **7**, 1403–1410.

2 O. Dukhno, F. Przybilla, M. Collot, A. Klymchenko, V. Pivovarenko, M. Buchner, V. Muhr, T. Hirsch and Y. Mély, *Nanoscale*, 2017, **9**, 11994–12004.

3 S. Lahtinen, A. Lyytikäinen, H. Päkkilä, E. Hömppi, N. Perälä, M. Lastusaari and T. Soukka, *J. Phys. Chem. C*, 2017, **121**, 656–665.

4 T. Mioduski, C. Gumiński and D. Zeng, *Journal of Physical and Chemical Reference Data*, 2014, **43**, 013105.

5 Y. Suzaki and A. Tachibana, Applied Optics, 1975, 14, 2809.

6 A. D. Edelstein, M. A. Tsuchida, N. Amodaj, H. Pinkard, R. D. Vale and N. Stuurman, *J Biol Methods*, , DOI:10.14440/jbm.2014.36.

7 S. Preibisch, S. Saalfeld and P. Tomancak, *Bioinformatics*, 2009, **25**, 1463–1465.

8 GDSC ImageJ Plugins : ImageJ : ... : Sussex Centre for Genome Damage and Stability : Lifesci : Schools : Staff : University of Sussex, http://www.sussex.ac.uk/gdsc/intranet/microscopy/imagej/gdsc_plugins, (accessed March 29, 2018).

9 S. Saalfeld, *mpicbg: Fiji module for image transformation and related algorithms*, 2018.

10 T. Mioduski, C. Gumiński and D. Zeng, *Journal of Physical and Chemical Reference Data*, 2015, **44**, 023102.

11 E. Mauerhofer, K. P. Zhernosekov and F. Rösch, *Radiochimica Acta*, 2009, **91**, 473–478.

12 A. Fick, *Journal of Membrane Science*, 1995, **100**, 33–38.

13 A. C. Lasaga, *Kinetic Theory in the Earth Sciences*, Princeton University Press, 2014.

14 C. K. Colton, K. A. Smith, E. W. Merrill and P. C. Farrell, *J. Biomed. Mater. Res.*, 1971, **5**, 459–488.